Supplementary Information

Hard carbon key properties allow for the achievement of high Coulombic efficiency and high volumetric capacity in Na-ion batteries

Adrian Beda [1,2], François Rabuel [3,4], Stephan Knopf [1,2], Mathieu Morcrette [3,4], Pierre-Louis Taberna [4,5], Patrice Simon [4,5], Camelia Matei Ghimbeu [1,2,4,*]

[1]*Université de Haute-Alsace, Institut de Science des Matériaux de Mulhouse (IS2M), CNRS UMR 7361, F-68100 Mulhouse, France*

[2]*Université de Strasbourg, F-67081 Strasbourg, France*

[3]*Université de Picardie Jules Verne, Laboratoire de Réactivité et Chimie des Solides (LRCS), UMR 7314 CNRS, HUB de l'Energie, 80039 Amiens, France*

[4]*Réseau sur le Stockage Electrochimique de l'Energie (RS2E), HUB de l'Energie, FR CNRS 3459, 80039 Amiens Cedex, France*

[5] *Université de Toulouse, CIRIMAT, UMR-CNRS 5085, F-31062 Toulouse, France*

Corresponding author:

*E-mail: camelia.ghimbeu@uha.fr

Results

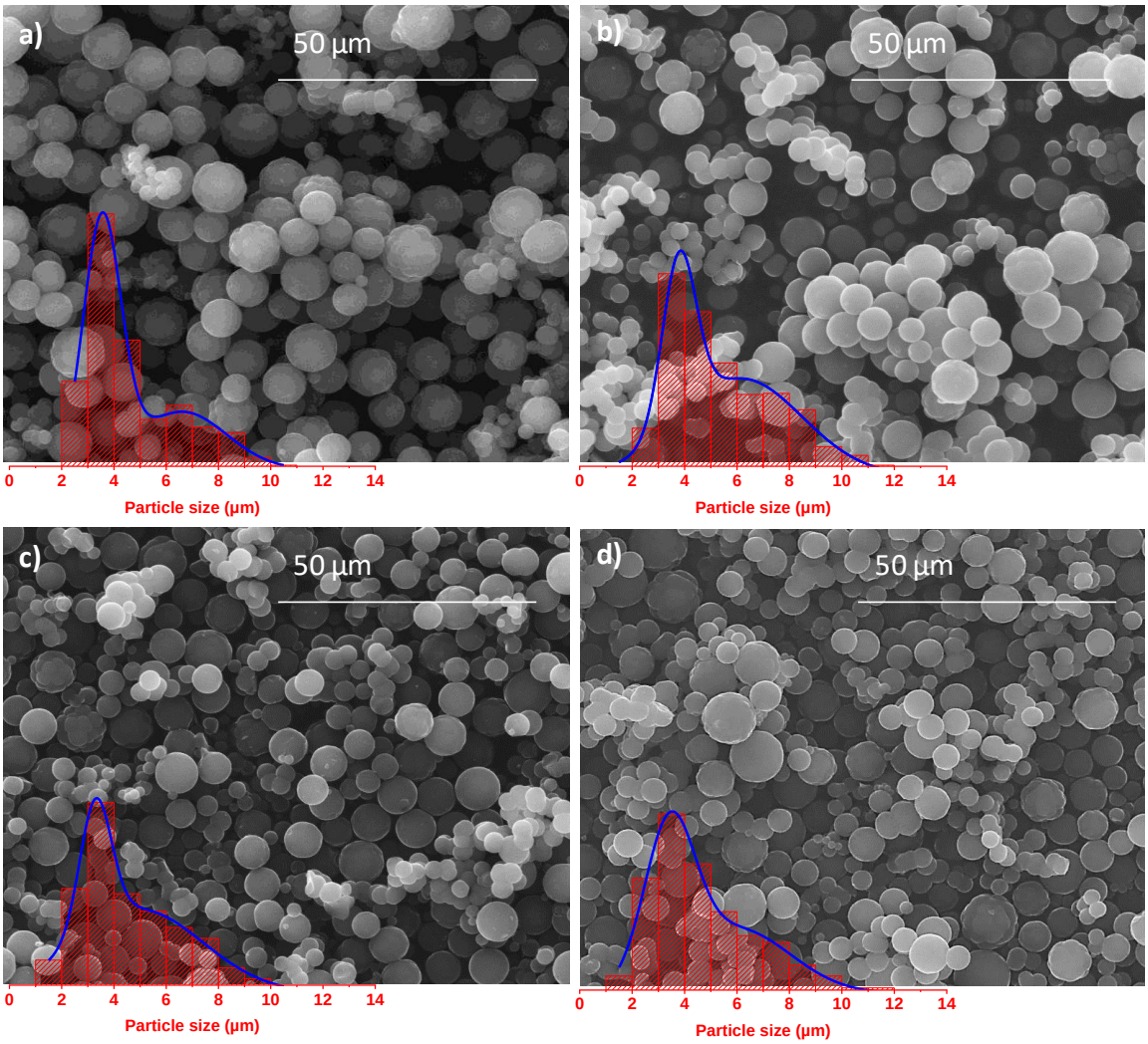

Figure S1. SEM of HCs spheres treated at a) 1300 °C, b)1400 °C, c) 1500 °C, d) 1600 °C along with the corresponding particle size distribution (inset).

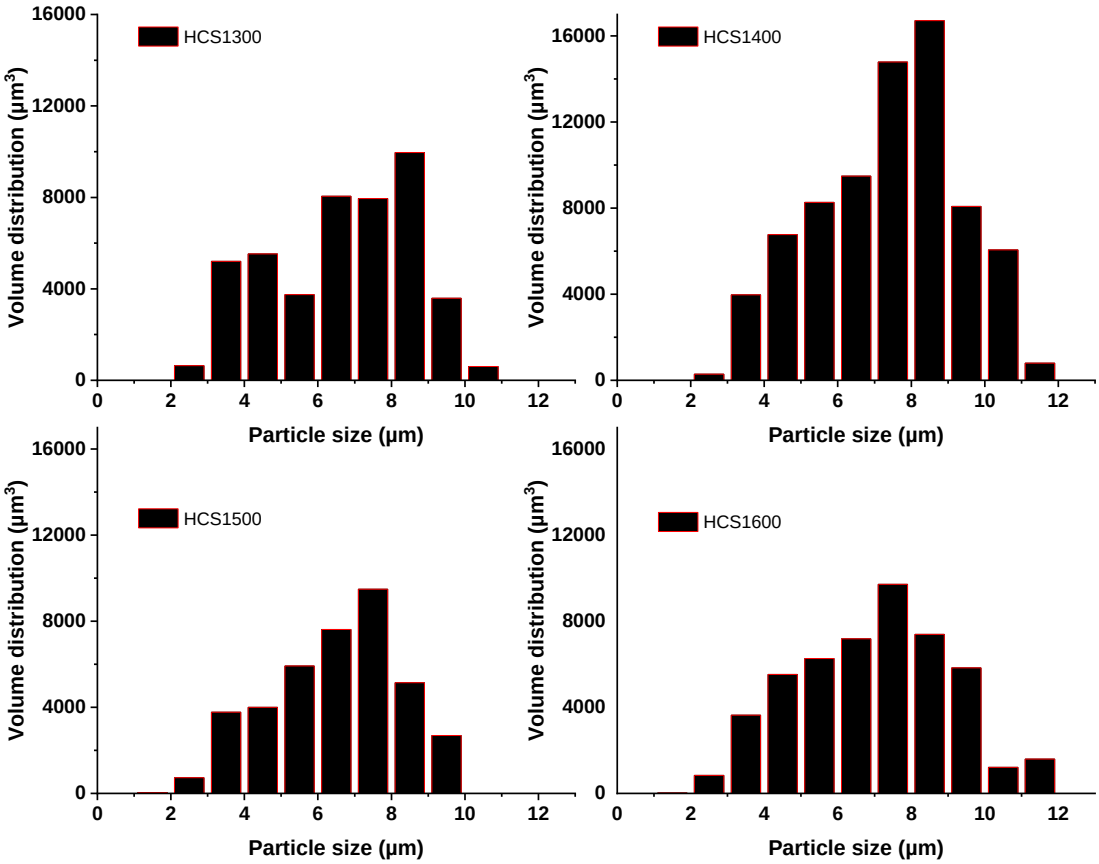

Figure S2. Volume distribution of the hard carbon spheres based on particle diameter and relative frequency, obtained through SEM images processing.

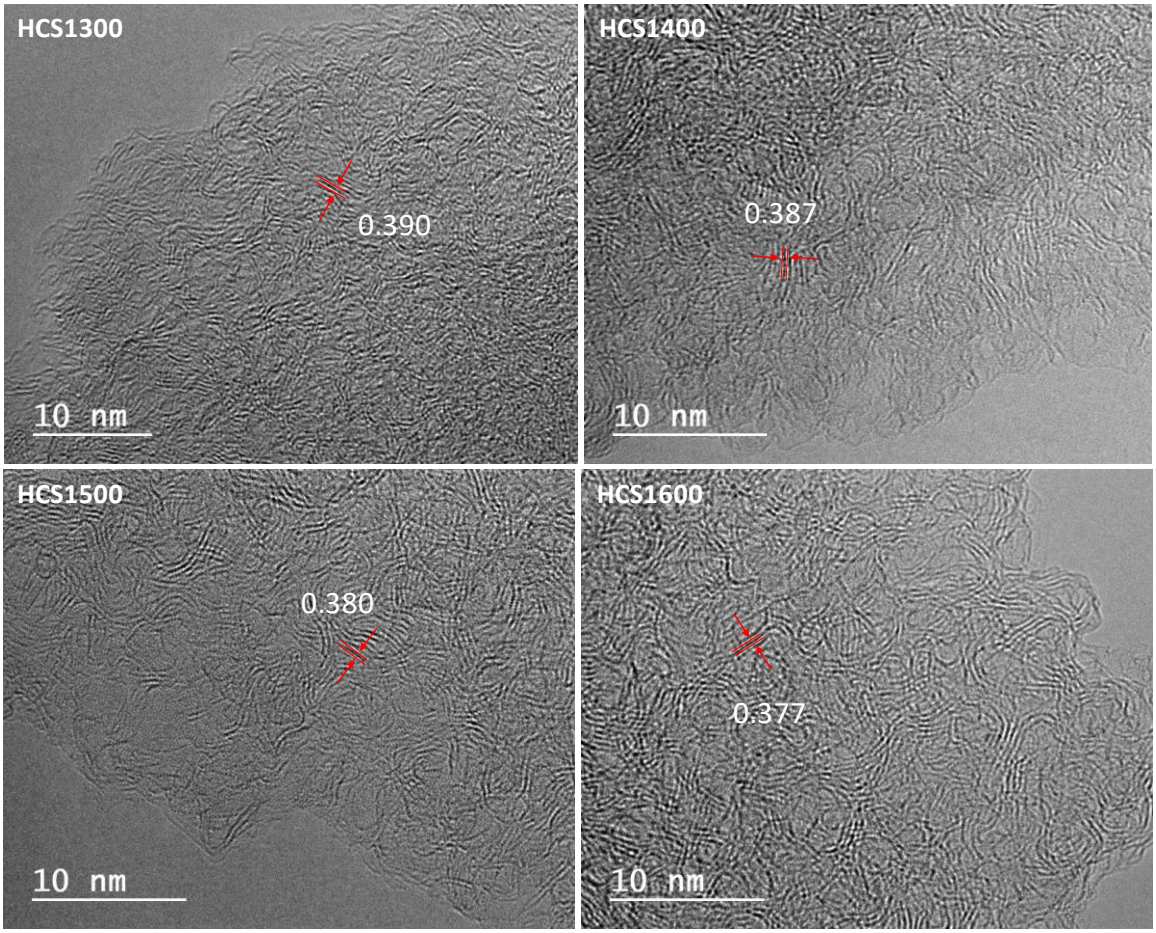

Figure S3. TEM images of hard carbon spheres treated at different temperatures

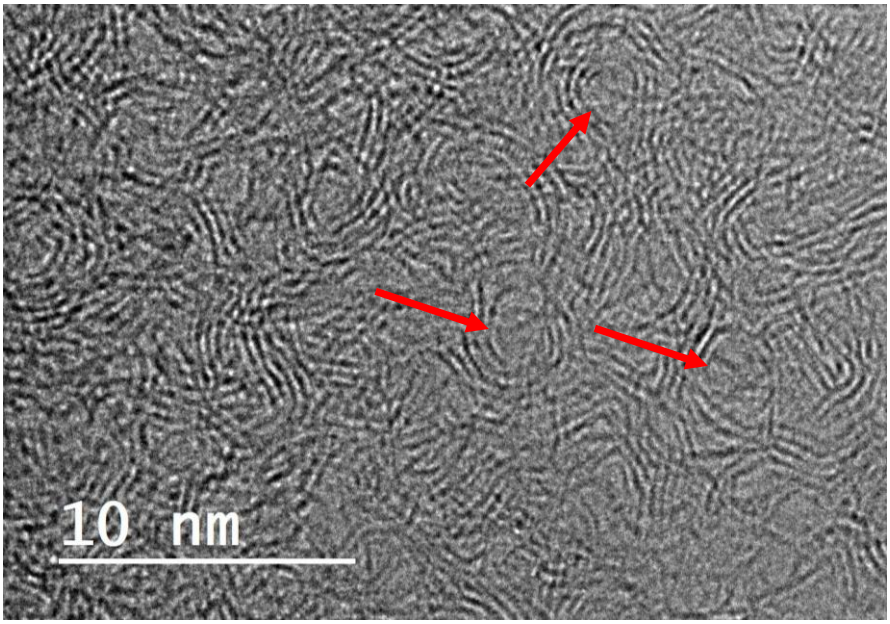

Figure S4. HR-TEM image of HCS1600 showing the presence of closed porosity

Table S1. Hard carbon structural properties determined by XRD: crystallite height and (Lc) crystallite length (La) and by Raman spectroscopy: the disorder degree obtained based on the FWHM and areal intensity of D and G bands.

Parameter	HCS1300	HCS1400	HCS1500	HCS1600
L_c	10.8	11.5	12.1	12.3
L_a	34.1	36.3	36.7	39.6
I_D/I_G	1.25	1.56	1.63	1.66
$FWHM_D/FWHM_G$	2.31	2.05	1.80	1.71

Table S2. Pycnometric (He) densities, total pore volumes determined by N_2 (V_{OP}), calculated volume ratios of closed porosity (R_{CP}), open porosity (R_{OP}) and solid phase for hard carbon materials studied.

HC	d_{He} (g cm^{-3})	V_{OP} N_2 (cm^3 g^{-1})	R_{CP} (%)	R_{OP} (%)	Solid phase (%)
HCS1300	2.10	0.0096	9.30	1.97	88.73
HCS1400	2.16	0.0073	6.79	1.55	91.66
HCS1500	1.87	0.0046	19.23	0.85	79.92
HCS1600	1.63	0.0069	29.41	1.11	69.48
PAC2	1.99	0.0102	13.73	1.95	84.30
PR1400	2.12	0.0164	8.33	3.35	88.30
TCA1400	1.95	0.0178	15.41	3.35	81.23
TCA1300	2.28	0.0728	1.47	14.23	84.28
HAB1400	2.22	0.0195	4.13	4.15	91.71

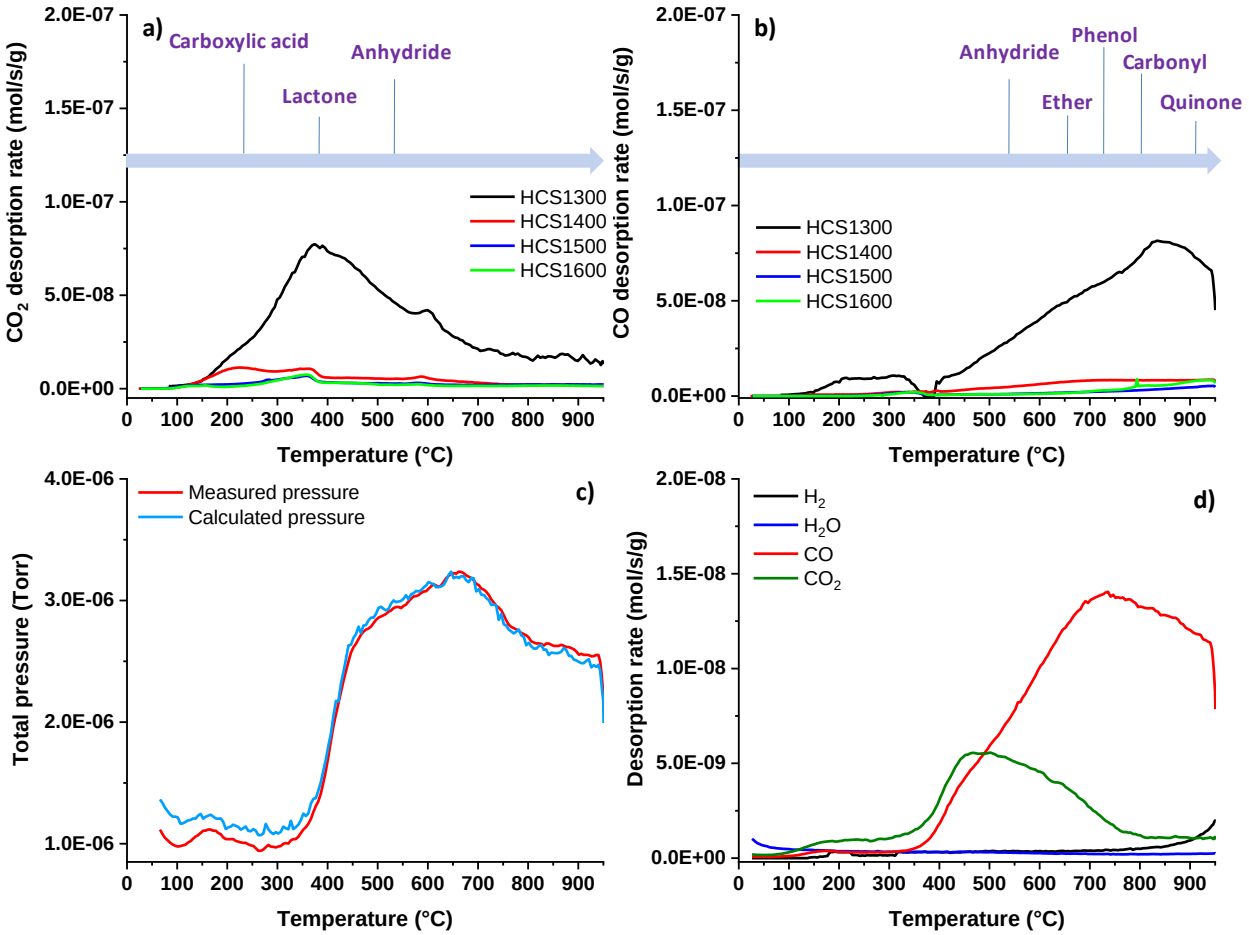

Figure S5. a) CO_2 and b) CO TPD-MS desorption curves along with the types of oxygen-based functional groups present on the carbon surface before their thermal decomposition, according to literature [1]. Example of active surface area measurement by TPD-MS for HCS1400: c) evolution of measured and calculated pressures and d) desorption profiles of the gases released during the ASA analysis.

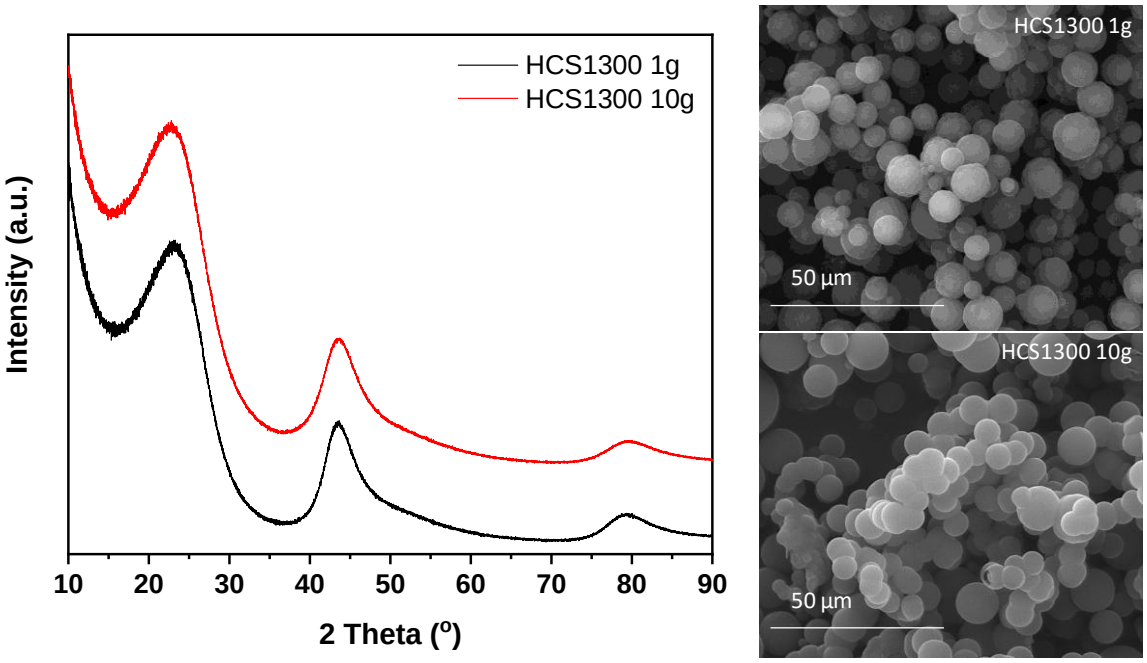

Figure S6. XRD spectra and SEM images of HCS1300 synthesized at lab-scale (1 g) and up-scale (10 g) which confirm the similar characteristics obtained.

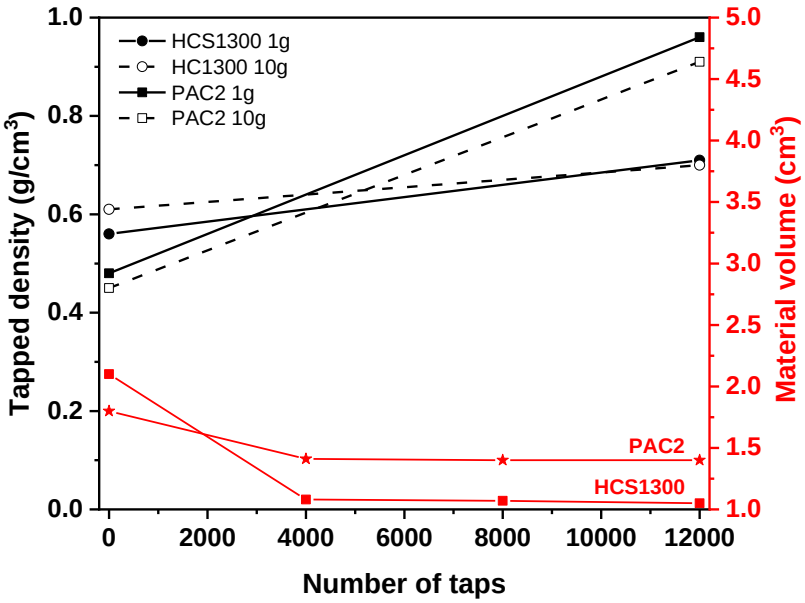

Figure S7. Hard carbon tapped density and volume evolution with the number of taps for HCS1300 vs. PAC2 commercial carbon.

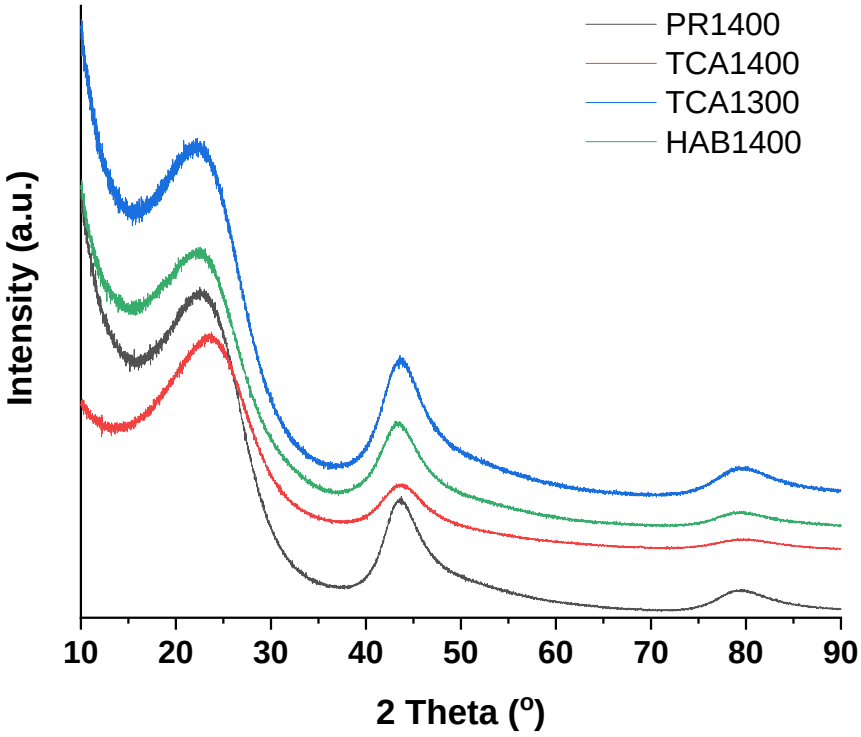

Figure S8. XRD diffractograms of the additional hard carbons discussed in the article.

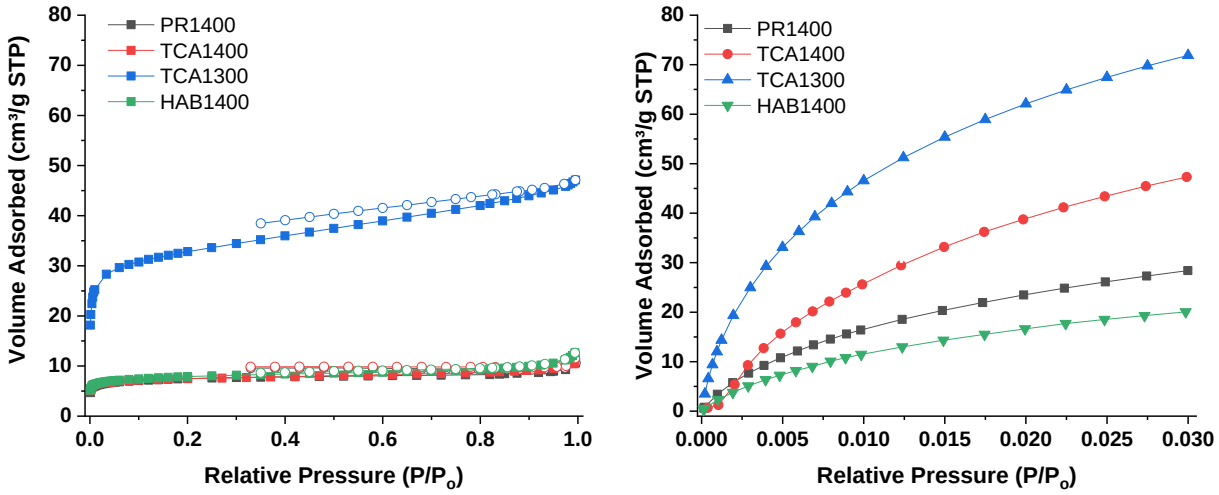

Figure S9. N_2 adsorption-desorption isotherms (left) and CO_2 adsorption isotherms (right) of the additional hard carbons approached in the study.

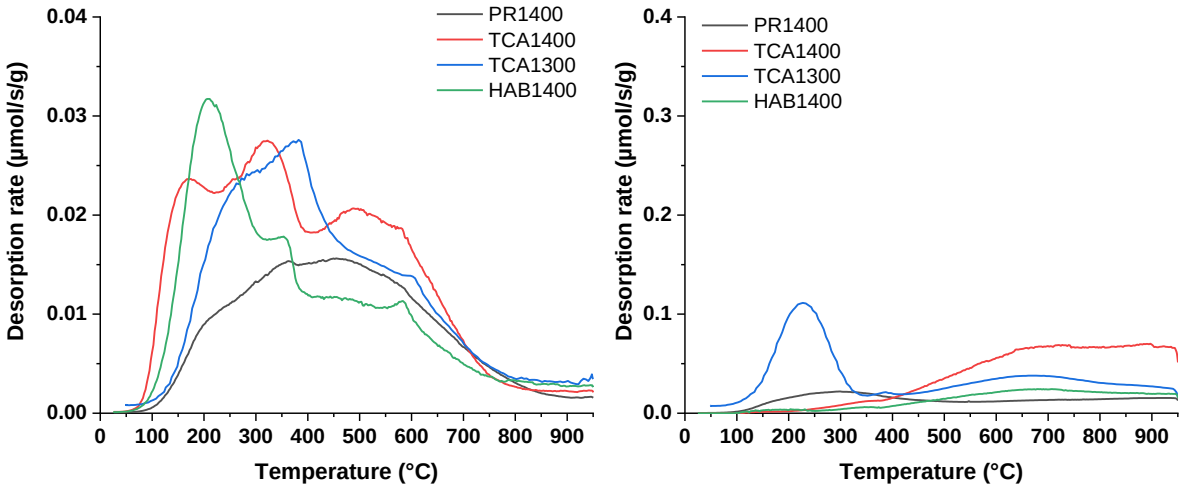

Figure S10. CO_2 (left) and CO (right) TPD-MS desorption curves of the additional carbons studied in the article.

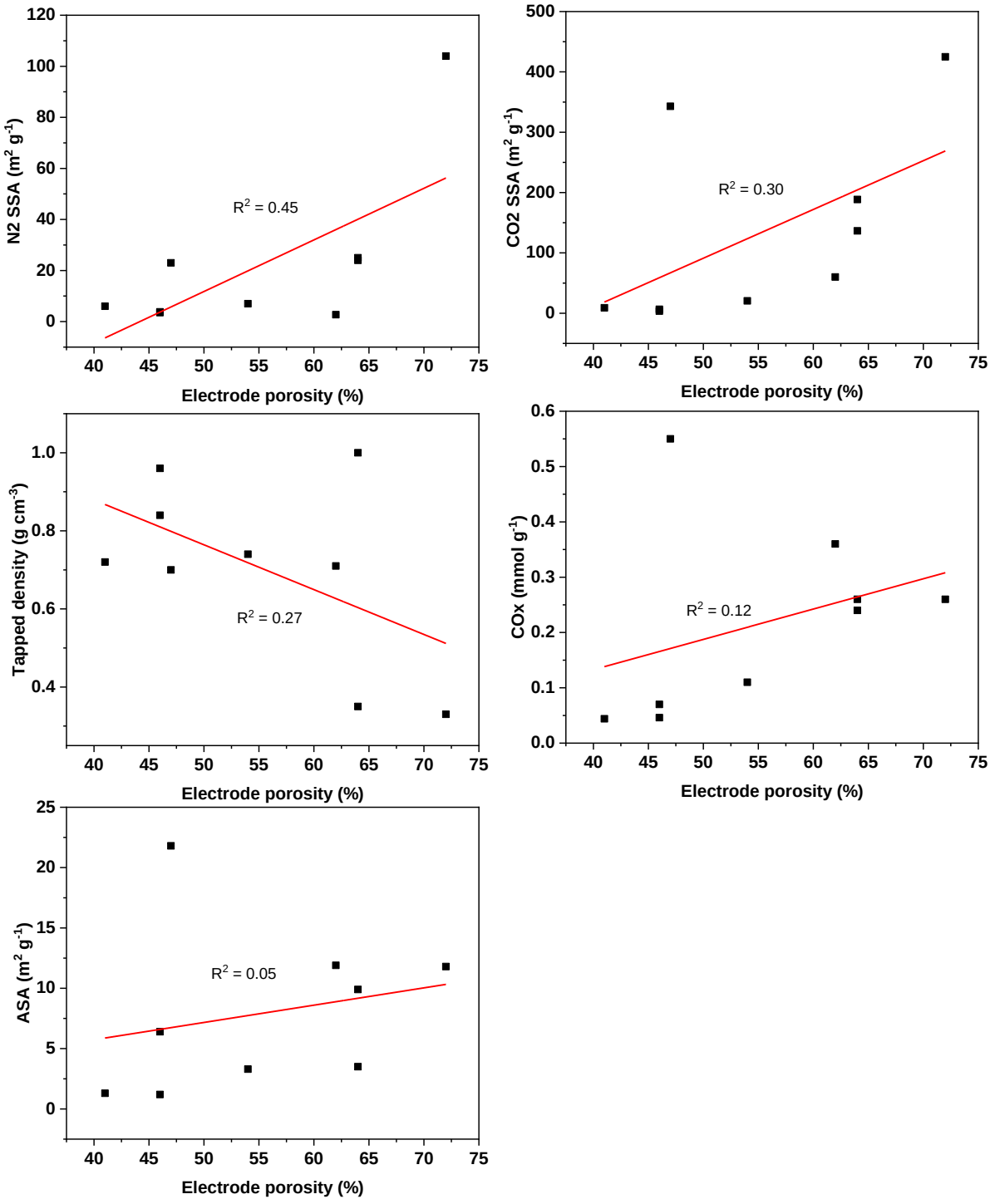

Figure S11. Electrode porosity represented as a function of different hard carbon properties. A linear fit was used to establish their correlation through the R^2 determination factor

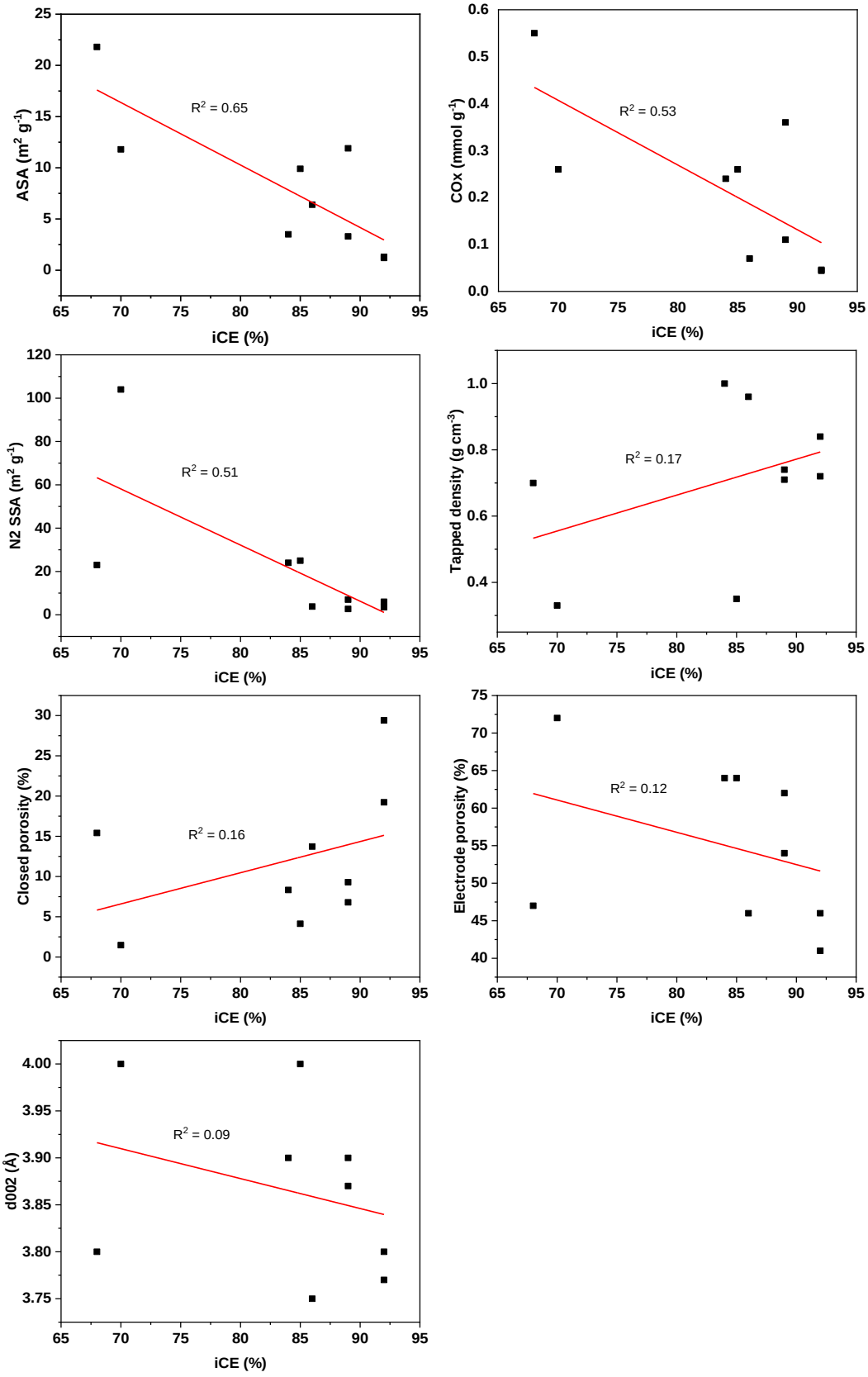

Figure S12. iCE correlations with different hard carbon characteristics/properties given by R^2 factor.

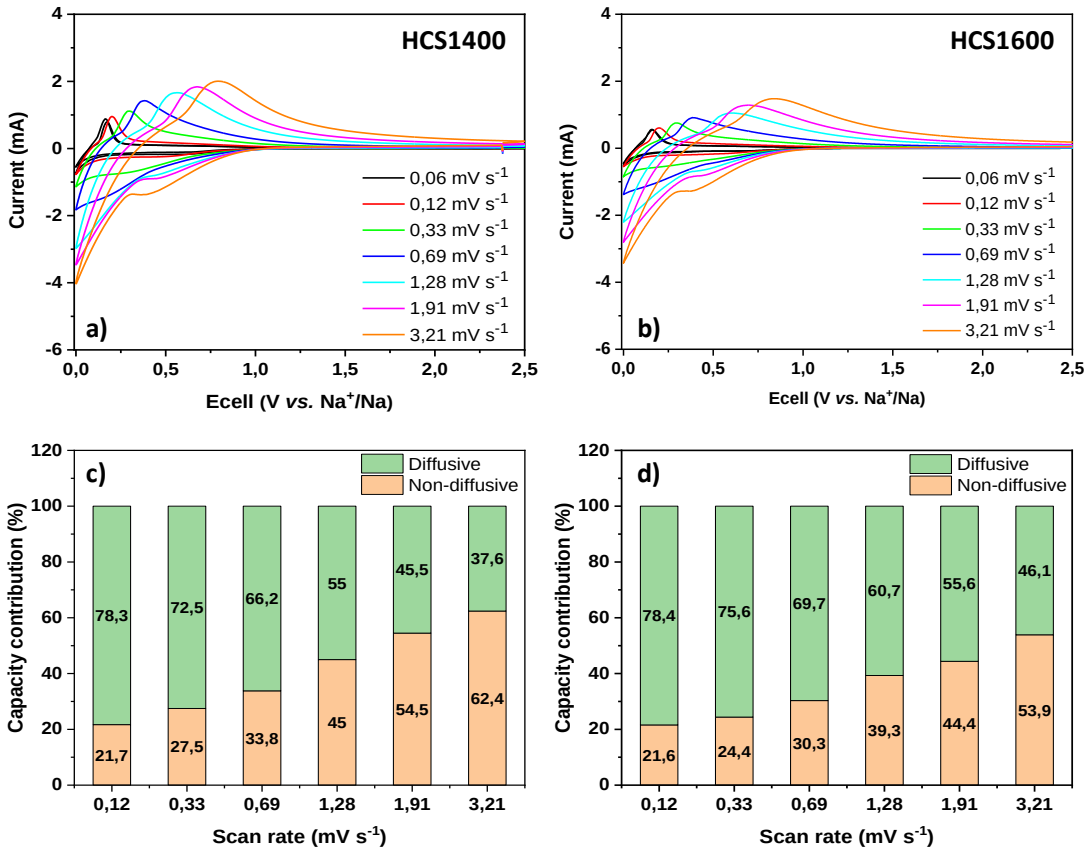

Figure S13. a-b) Cyclic voltammograms at different scan rates (0.06–3.2 mV s^{-1}) between 0 V and 2.5 V *vs.* Na^+/Na for HCS1400 and HCS1600. c-d) The diffusive and non-diffusive contribution at different scan rate of HCS1400 and HCS1600 respectively.

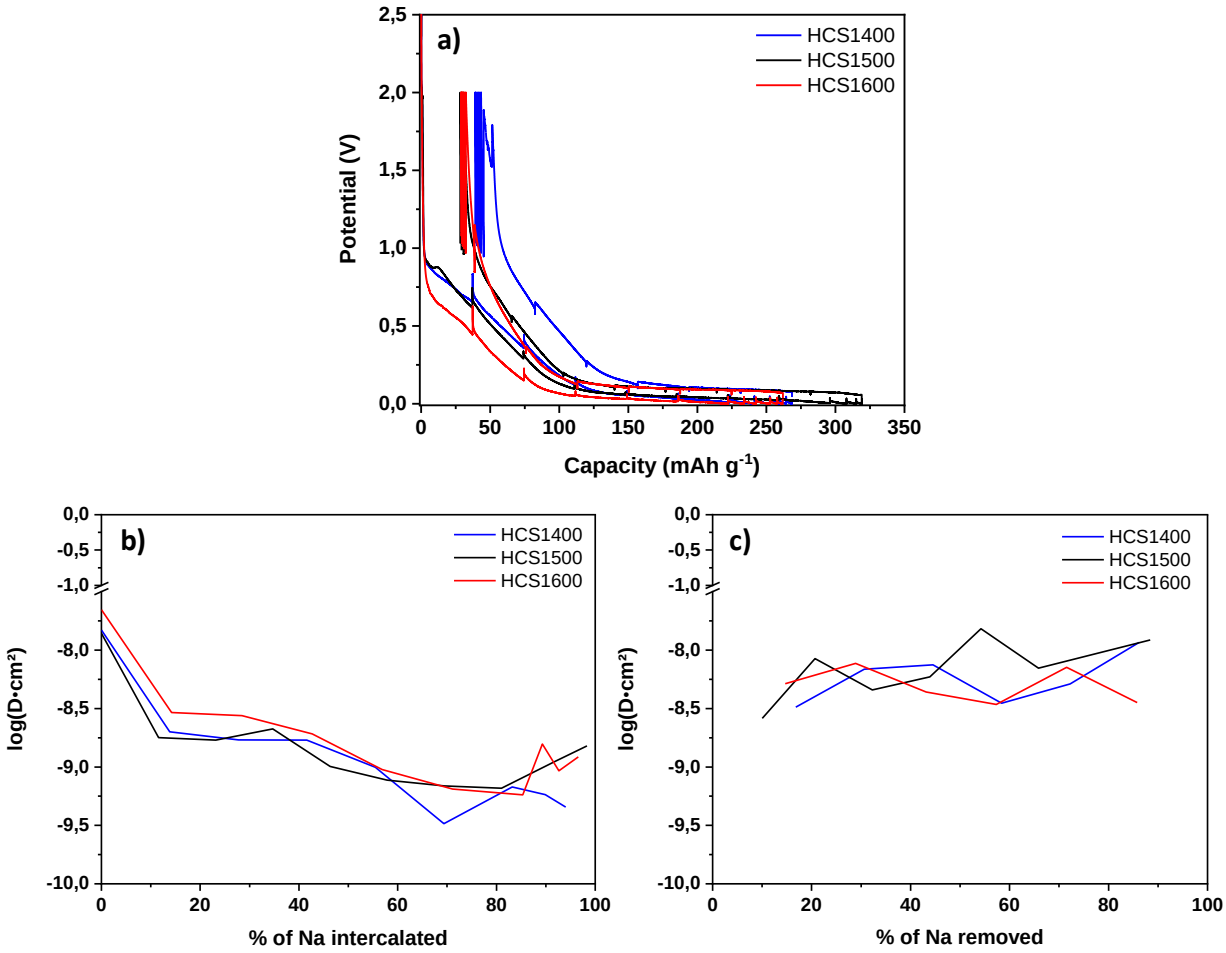

Figure S14. a) GITT potential profiles of sodiation and desodiation of HC materials during the first cycle. Sodium-ion apparent diffusion coefficients estimated during b) sodium intercalation and c) sodium extraction.

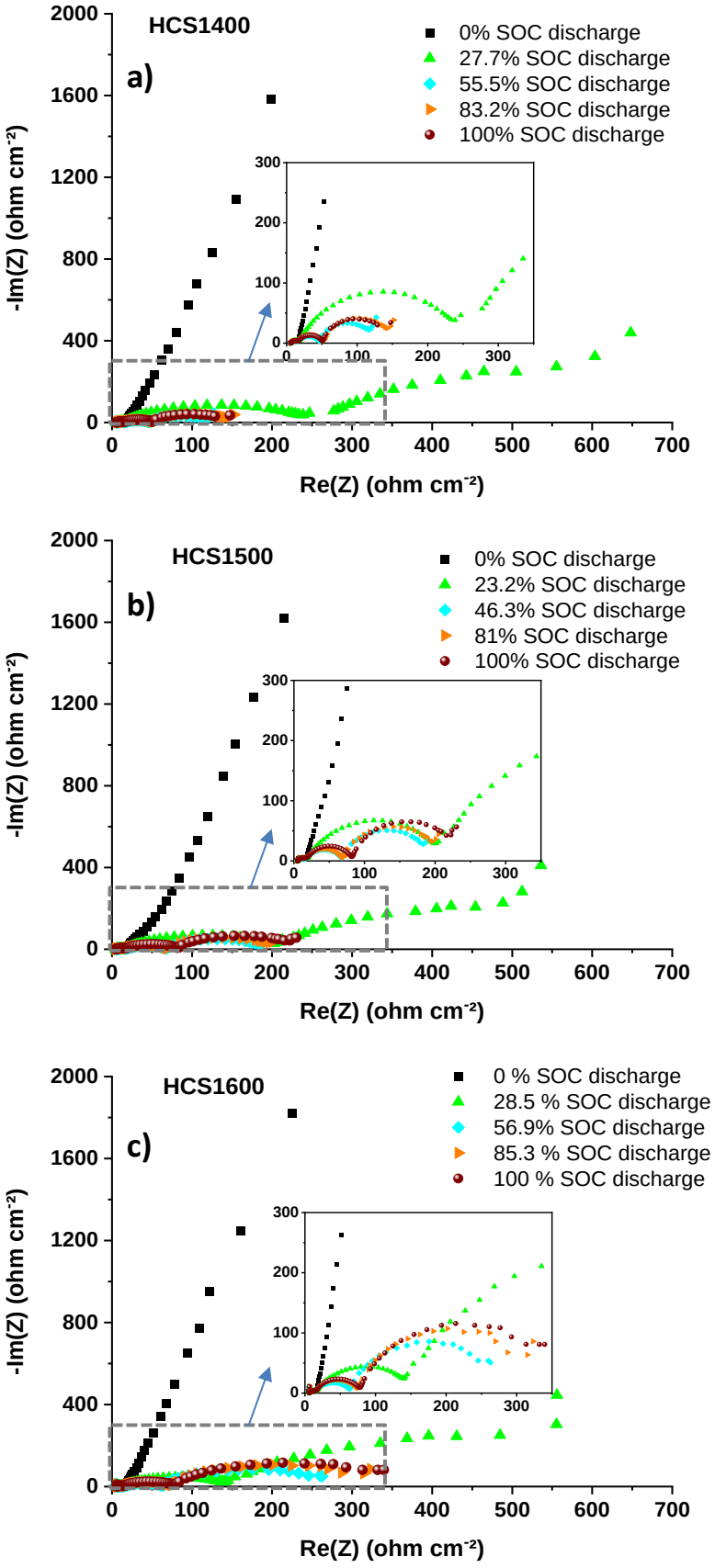

Figure S15. Electrochemical impedance spectra of HCS1400, HCS1500 and HCS1600 at different states of charge (SOC) during sodiation. The measurements were done in half-cells *vs.* Na.

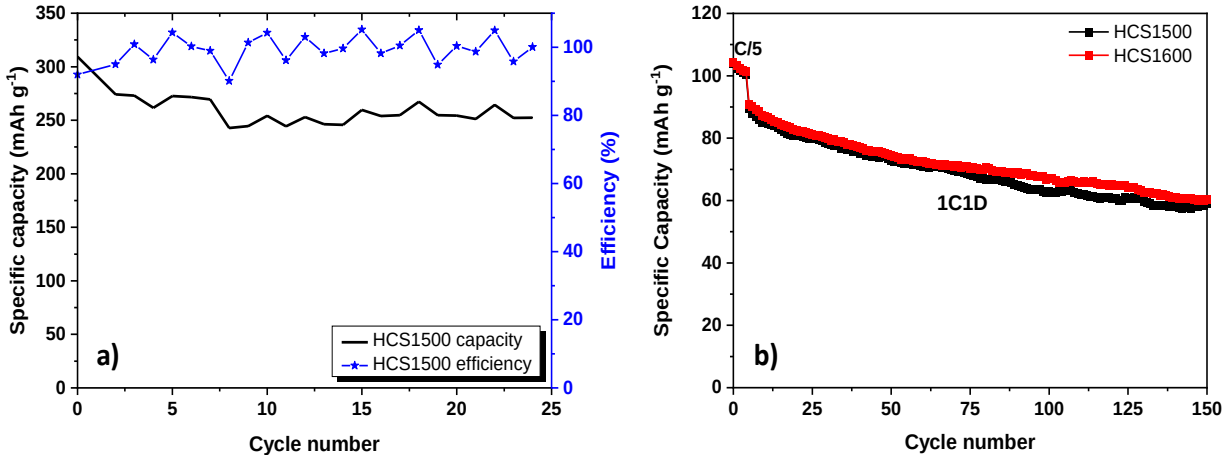

Figure S16. a) Specific capacity evolution with the cycle number of HCS1500 in half-cell *vs.* Na and b) Specific capacity over cycling for HCS1500 and HCS1600 in full-cell *vs.* NVPF at 1C1D rate.

Table S3. Electrochemical performance of full-cells sodium systems based on HC anode and different cathode materials reported in the literature.

Anode Material	Cathode Material	iCE %	C-rate	Capacity mAh g^{-1}	Refference
HC	$Na_3V_2(PO_4)_2F_3$	86	C/10 1C	107 70	This paper
HC	$NaNi_{0.5}Ti_{0.5}O_2$	65	10 mA g^{-1}	82	[2]
HC	$Na_3Fe_2(PO_4)_3$	-	10 mA g^{-1}	98.3	[3]
HC	$Na_3V_2(PO_4)_2F_3$	55	C/20	110	[4]
HC	$Na_{1-y}(Ni_{1/3}Fe_{1/3}Mn_{1/3})O_2$	72	15 mA g^{-1}	125	[5]
HC	$Na_{2/3}Ni_{1/3}Mn_{2/3}O_2$	-	25 mA g^{-1}	70	[6]
HC	$Na_{0.44}MnO_2$	57	12.1 mA g^{-1} 60.5 mA g^{-1}	120 105	[7]
HC	$Na(Cu_{1/9}Ni_{2/9}Fe_{1/3}Mn_{1/3})O_2$	75	C/10	100	[8]
HC	$Na_{0.9}FePO_4$	85	20 mA g^{-1}	126	[9]

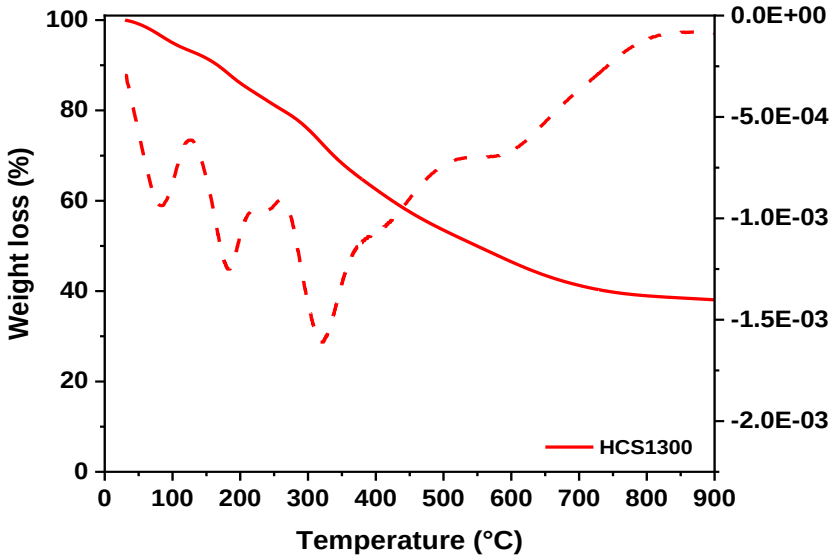

Figure S17. TGA and DTG analysis of HCS1300 polymer spheres (before carbonization) under inert gas (N_2)

Experimental details

Materials synthesis.

Hydrothermal carbonization (HTC) was used to prepare **HAB1400** material, starting from glucose precursor. A solution of 0.8 M concentration was prepared by mixing 250 mL of water with the corresponding amount of glucose, placed in a stainless-steel autoclave and heated up to a temperature of 180 °C for 20h. Next, the autoclave was removed from the oven and let to naturally cool down. The solid formed denoted as hydrochar was collected, dried overnight at 80 °C and then heat treated at 1400 °C under Ar for 1h (heat rate of 5 °C/min) to obtain the hard carbon (HAB1400).

TCA1300 and TCA1400 hard carbons were prepared in a similar way as described in the main manuscript, however, some supplementary precursors were used in order to modify the particle size and properties. This procedure involved therefore, simple dissolution of phloroglucinol (1.64 g) and glyoxylic acid (1.44 g) in presence of water followed by the addition of 0.72 mL of TCA (thiophene carboxaldehyde). After few minutes of stirring, 0.72 g of L-Cysteine and 0.72 g of TEDA were added. The solution was next left on an oil bath for 24h. As in the previous case, the solid is recovered and dried overnight at 80 °C then

pyrolyzed at 1300°C and 1400 °C, respectively under Ar flow to obtain the hard carbons (TCA1300 and TCA1400).

PR1400 was obtained by polymerization of phloroglucinol and glyoxylic acid in ethanol solvent in a similar manner as described in our previous work [10]. No TEDA was used to obtain a random morphology instead of spherical one.

$Na_3V_2(PO_4)_2F_3$

The synthesis of $Na_3V_2(PO_4)_2F_3$ followed a multi-step procedure adapted from the patent of Barker et al. [11]. Briefly, H_3PO_4 was stirred in presence of water, V_2O_5 and agar-agar ($C_{14}H_{24}O_9$). Next, the solution was dried at low temperature until the solvent was removed and the mixture was treated at 250 °C under O_2 for 2h. In the next step, the recovered material was heat-treated in inert atmosphere at 890 °C for 2h. The resulting product, VPO_4, was further mixed with NaF and heat-treated at 700 °C for 1h30, under inert atmosphere, resulting in the formation of NVPF material.

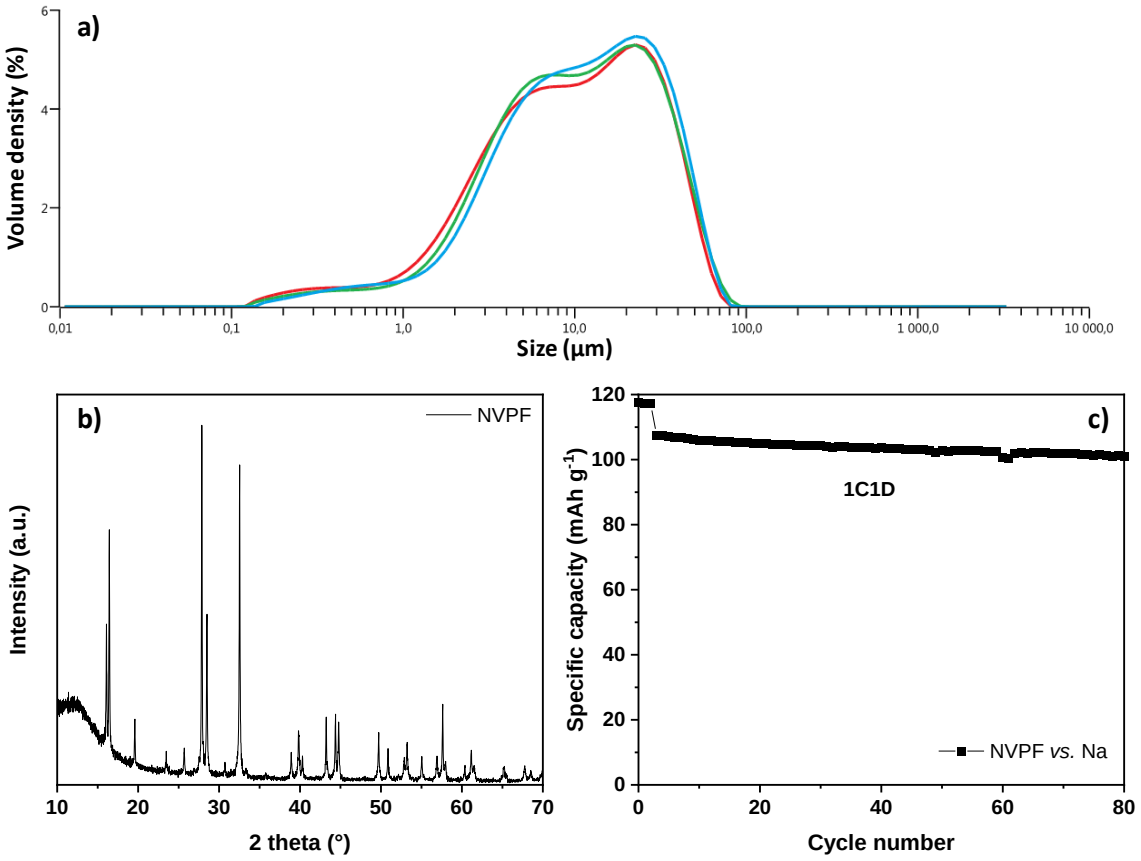

Figure S18. a) Granulometric analysis of NVPF material along with the b) XRD diffractogram. c) Electrochemical performance of NVPF *vs.* Na metallic at 1C1D rates.

References

1 G. Moussa, C. Matei Ghimbeu, P.-L. Taberna, P. Simon and C. Vix-Guterl, *Carbon*, 2016, **105**, 628–637.

2 H. Wang, Y. Xiao, C. Sun, C. Lai and X. Ai, *RSC Adv.*, 2015, **5**, 106519–106522.

3 Y. Cao, Y. Liu, D. Zhao, X. Xia, L. Zhang, J. Zhang, H. Yang and Y. Xia, *ACS Sustainable Chem. Eng.*, 2020, **8**, 1380–1387.

4 A. Ponrouch, R. Dedryvère, D. Monti, A. E. Demet, J. M. A. Mba, L. Croguennec, C. Masquelier, P. Johansson and M. R. Palacín, *Energy Environ. Sci.*, 2013, **6**, 2361–2369.

5 D. Kim, E. Lee, M. Slater, W. Lu, S. Rood and C. S. Johnson, *Electrochemistry Communications*, 2012, **18**, 66–69.

6 M. Dahbi, M. Kiso, K. Kubota, T. Horiba, T. Chafik, K. Hida, T. Matsuyama and S. Komaba, *J. Mater. Chem. A*, 2017, **5**, 9917–9928.

7 Y. Liu, X. Liu, F. Bu, X. Zhao, L. Wang, Q. Shen, J. Zhang, N. Zhang, L. Jiao and L.-Z. Fan, *Electrochimica Acta*, 2019, **313**, 122–130.

8 Y. Zheng, Y. Lu, X. Qi, Y. Wang, L. Mu, Y. Li, Q. Ma, J. Li and Y.-S. Hu, *Energy Storage Materials*, 2019, **18**, 269–279.

9 Z. Zhang, Y. Du, Q.-C. Wang, J. Xu, Y.-N. Zhou, J. Bao, J. Shen and X. Zhou, *Angewandte Chemie International Edition*, 2020, **59**, 17504–17510.

10 A. Beda, P.-L. Taberna, P. Simon and C. Matei Ghimbeu, *Carbon*, 2018, **139**, 248–257.

11 United States, US6387568B1, 2002.